BIOCHEMISTRY
including biophysical chemistry & molecular biology
Article

Biochemistry **2009,** *48,* 7629–7635 7629
DOI: 10.1021/bi900756y

A Novel β-Defensin Structure: Big Defensin Changes Its N-Terminal Structure To Associate with the Target Membrane[†,‡]

Takahide Kouno,[§] Mineyuki Mizuguchi,*[,§] Tomoyasu Aizawa,[∥] Hiroyuki Shinoda,[§] Makoto Demura,[∥] Shun-ichiro Kawabata,[⊥] and Keiichi Kawano[∥]

[§]*Faculty of Pharmaceutical Sciences, University of Toyama, Toyama 930-0194, Japan,* [∥]*Division of Biological Sciences, Graduate School of Science, Hokkaido University, Sapporo 060-0810, Japan, and* [⊥]*Department of Biology, Kyushu University, Fukuoka 812-8582, Japan*

Received May 1, 2009; Revised Manuscript Received July 7, 2009

ABSTRACT: Big defensin is a 79-residue peptide derived from hemocytes of the Japanese horseshoe crab. The amino acid sequence of big defensin is divided into an N-terminal hydrophobic domain and a C-terminal cationic domain, which are responsible for antimicrobial activities against Gram-positive and -negative bacteria, respectively. The N-terminal domain of big defensin forms a unique globular conformation with two α-helices and a parallel β-sheet, while the C-terminal domain adopts a β-defensin-like fold. Although our previous study implied that big defensin changes its N-terminal structure in a micellar environment, due to the poor quality of the NMR spectra it remained to be resolved whether the N-terminal domain adopts any structure in the presence of micelles. In this analysis, we successfully determined the structure of the N-terminal fragment of big defensin in a micellar solution, showing that the fragment peptide forms a single α-helix structure. Moreover, NMR experiments using paramagnetic probes revealed that the N-terminal domain of big defensin penetrates into the micelle with a dipping at the N-terminal edge of the α-helix. Here, we propose a model for how big defensin associates with the target membrane.

A variety of antimicrobial peptides have been discovered so far, and they play a fundamental role in the innate immunity of invertebrates and vertebrates (*1*, *2*). Defensins make up a major group of antimicrobial peptides and have relatively short amino acid sequences with cationic net charges and three intramolecular disulfide bonds (*3*, *4*). Defensin molecules are classified into subfamilies according to their disulfide patterns: for example, the six half-cystines are linked in the 1−6, 2−4, and 3−5 pattern for α-defensin and the 1−5, 2−4, and 3−6 pattern for β-defensin. Despite the different disulfide patterns, α- and β-defensin have a similar three-dimensional structure that consists of a triple-stranded β-sheet assisted by three disulfide bonds (*1*, *3*, *4*). Both defensins are cationic and bind via electrostatic interactions directly to target bacterial membranes as they contain phospholipids with negatively charged headgroups (*5*). In addition, many α- and β-defensins have reduced antimicrobial activities in the presence of a high concentration of salt (*3*, *4*). Some groups have shown that defensin interacts with a negatively charged model membrane (*6*−*9*). Although it is not clear how defensin binding to bacterial membranes leads to the death of microorganisms, defensin may form a transmembrane pore, resulting in permeabilization of the target membrane (*6*, *8*, *9*).

Interestingly, bacteria also produce antimicrobial peptides, generally termed bacteriocins, which are more potent than those produced by plants and animals; for example, pediocin-like (class IIa) bacteriocins are produced by a variety of lactic acid bacteria (*10*, *11*). In membrane-mimicking environments, pediocin-like bacteriocins form a triple-stranded β-sheet or β-sheet-like structure in the N-terminal region, whereas the C-terminal half includes a hydrophobic/amphiphilic α-helix structure and an extended tail (*11*). Site-directed and chimera mutation analyses using sakacin P, a member of the group of pediocin-like peptides, indicated that the C-terminal region plays a major role in antimicrobial activity and target specificity (*12*, *13*). The hydrophobic/amphiphilic C-terminal domain of pediocin-like bacteriocins has been reported to penetrate into the hydrophobic core of the membrane, leading to destabilization of the target cell membrane and leakage of intracellular components (*11*).

We have explored the immunity of the Japanese horseshoe crab (*Tachypleus tridentatus*; known as "kabutogani" in Japanese) and identified a variety of immunity-related factors (*14*, *15*). In the horseshoe crab, the hemocytes that are responsible for the innate immunity release many immunity-related factors into the extracellular space immediately after stimulation, such as by recognition of lipopolysaccharides, outer membrane components of Gram-negative bacteria (*16*, *17*). The immunity-related factors include coagulation factors, protein inhibitors, antimicrobial peptides, and lectins that are induced to kill invading microbes and prevent leakage of the hemolymph (*14*, *15*). Big defensin is also secreted from the hemocytes and has antimicrobial activities against Gram-positive and -negative bacteria and fungi (*18*). The 79-amino acid sequence of big defensin is divided into two

[†]This study was supported by grants from the Ministry of Education, Culture, Sports, Science and Technology of Japan (MEXT), by the National Project on Protein Structural and Functional Analyses (MEXT), and by the Program for the Promotion of Basic Research Activities for Innovative Biosciences (PROBRAIN).

[‡]The ^{1}H chemical shifts and atomic coordinates of big-N peptide were deposited in the BioMagResBank as entry 11072 and the Protein Data Bank as entry 2RQ2, respectively.

*To whom correspondence should be addressed: Faculty of Pharmaceutical Sciences, University of Toyama, Toyama 930-0194, Japan. Telephone: +81-76-434-7595. Fax: +81-76-434-5061. E-mail: mineyuki@pha.u-toyama.ac.jp.

Published on Web 07/09/2009

regions, the highly hydrophobic N-terminal half and the cationic C-terminal half. Intriguingly, these two regions can be separated by trypsin cleavage, and the antimicrobial activities can be divided into the two domains; activity against Gram-positive and -negative bacteria is derived from the N-terminal and C-terminal fragments of big defensin, respectively (*18*).

We previously resolved the solution structure of big defensin and demonstrated that the C-terminal domain forms a β-sheet structure with three disulfide bonds just like the β-defensin structure, whereas the N-terminal domain adopts a unique globular conformation consisting of a parallel β-sheet and two α-helices (*19*). Intriguingly, circular dichroism (CD)[1] and nuclear magnetic resonance (NMR) data indicated that the hydrophobic N-terminal domain undergoes a conformational change in a micellar environment, resulting in a disruption of the parallel β-sheet structure. However, the structure of big defensin bound to micelles remains to be resolved. In this study, we successfully determined the solution structure of the N-terminal fragment of big defensin in sodium dodecyl sulfate (SDS) micelles and observed the association of the fragment peptide with the micelles using paramagnetic probes. These results provide a picture of how the N-terminal domain is used by big defensin to recognize the target cell membrane.

EXPERIMENTAL PROCEDURES

Peptide. The N-terminal fragment corresponding to residues P5−N34 of a mature big defensin, termed big-N, was synthesized by Toray Research Center (Tokyo, Japan). Matrix-assisted laser desorption time-of-flight mass spectrometry gave a main peak with a molecular weight of 2887.5 (the calculated weight of the target peptide is 2887.3) and some peaks with much lower intensities (data not shown). Further purification was not performed because the insolubility of the peptide makes its purification difficult. The minor components produce few signals on NMR spectra; thus, interference with the structural determination of big-N was unlikely. The big-N peptide powder was added to aqueous buffer (components described below), and the mixture was sonicated for 10 min. After centrifugation at 15000*g* for 5 min, the supernatant was used for all experiments. Big-N concentrations were estimated according to the absorbance at 280 nm, and the molar extinction coefficient was based on the number of tyrosine and tryptophan residues in the peptide ($\varepsilon = 8480\ M^{-1}\ cm^{-1}$) (*20*).

CD Spectroscopy. All CD spectra were recorded on a Jasco J-805 spectropolarimeter with a 1.0 mm quartz cell at 30 °C. Big-N peptide was dissolved in aqueous buffer [50 mM acetic acid (pH 3.5), 20 mM NaCl, and 0.3−10 mM SDS or DPC] at a final concentration of 10 μM. The CD spectra of all samples were corrected using reference samples of similarly prepared solutions in the absence of the peptide. Ellipticity was reported as the mean residue molar ellipticity.

NMR Spectroscopy. Big-N peptide was dissolved in 250 μL of aqueous buffer [50 mM deuterated acetic acid-d_4 (pH 3.5), 20 mM NaCl, 100 mM deuterated SDS-d_{25}, and 5 or 100% D_2O]. For experiments using paramagnetic probes, 3 mM 16-doxyl-stearic acid (16-Dox), 0.5 mM $MnCl_2$, or 0.5 mM $MnCl_2$ and 5 mM ethylenediamine-*N*,*N*,*N*′,*N*′-tetraacetic acid (EDTA) disodium salt were added to the buffer prior to big-N powder being dissolved. The NMR sample was centrifuged at 15000*g* for 5 min to remove aggregated peptide, and the peptide concentration of the supernatant was estimated to be 0.30−0.35 mM. All of the NMR spectra were recorded at 303 K on a Bruker AV800 spectrometer equipped with a cryogenic probe. DQF-COSY (*21*), TOCSY (mixing times of 50 and 75 ms) (*22*), and NOESY (60, 80, 100, 120, 140, and 160 ms) (*23*) spectra were acquired with solvent suppression using the WATERGATE sequence (*24*). The DQF-COSY spectrum was recorded with 4096 × 512 data points, and the other spectra were recorded with 2048 × 512 data points and 96 scans. ^{1}H chemical shifts were directly referenced to the resonance of 2,2-dimethyl-2-silapentane-5-sulfonate sodium salt. The assignments of ^{1}H resonances of the backbone and the side chains were made using a series of two-dimensional NMR experiments as described previously (*25*). The $^3J_{HNH\alpha}$ coupling constants derived from the DQF-COSY spectrum were used for estimation of dihedral angles (ϕ) according to the Karplus equation. Furthermore, 1 h after big-N peptide had been dissolved in 100% D_2O buffer, slowly exchanging amide protons were identified from the TOCSY spectrum. To identify and quantify the signal attenuation by the paramagnetic probes, TOCSY spectra were recorded in the absence and presence of the paramagnetic reagents, and the peak intensities were compared. For severely overlapped signals, the corresponding data were excluded from the analysis. All NMR spectra were processed and analyzed with NMRPipe (*26*) and Sparky (*27*).

Structure Calculations. For structure calculations of big-N, distance restraints were collected from two-dimensional homonuclear NOESY spectra acquired with a mixing time of 120 ms in 5 or 100% D_2O buffer. The assignments of NOE cross-peaks and structure calculations were performed iteratively and manually. The interproton distance (r) was derived from the NOE intensity (S) with the relationship $r = c(S)^{-6}$, where c is a coefficient determined on the basis of NOE corresponding to a known distance. For the NOESY spectra in a 5% D_2O solution, $H^N(i)-H^\alpha(i-1) = 1.70-3.60$ Å and $H^N(i)-H^\alpha(i) = 2.70-3.50$ Å for residues in the α-helix; for the NOESY spectra in a 100% D_2O solution, $H^\alpha-H^\beta = 2.50-2.70$ Å for alanine. A 50% error on the peak intensities was assumed, and the estimated interproton distance was used as an upper bound. For all interproton restraints, the lower bound was set to 1.80 Å. The hydrogen bonds were identified according to amide protons that exchanged slowly with the solvent deuterium, and their partners were assigned on the basis of the early structure calculations. For hydrogen bonds, distance restraints of 2.30−3.30 and 1.30−2.30 Å were used for N−O and H^N−O atom pairs, respectively. The restraints for the hydrogen bonds and the dihedral angles were incorporated into the late stage of structure calculations. Finally, a simulated annealing protocol was applied using 12000 steps at a high temperature (1000 K) and 8000 steps for the cooling process. A total of 50 structures were calculated, and the 20 lowest-energy structures were used for calculation of the energy-minimized average structure. The quality of the obtained structure was analyzed with MOLMOL (*28*) and PROCHECK-NMR (*29*). Structural figures were generated with MOLMOL. Detailed experimental data and structural statistics are summarized in Table 1.

[1]Abbreviations: 16-Dox, 16-doxyl-stearic acid; CD, circular dichroism; DQF-COSY, double-quantum-filtered correlation spectroscopy; DPC, dodecylphosphocholine; EDTA, ethylenediamine-*N*,*N*,*N*′,*N*′-tetraacetic acid; NMR, nuclear magnetic resonance; NOE, nuclear Overhauser enhancement; NOESY, NOE spectroscopy; rmsd, root-mean-square deviation; SDS, sodium dodecyl sulfate; TOCSY, total correlation spectroscopy.

Table 1: Structural Statistics for the 20 Lowest-Energy Structures of Big-N

no. of distance restraints	
NOE-derived distance restraints	
total	266
intraresidue ($\|i-j\| = 0$)	125
sequential ($\|i-j\| = 1$)	95
medium-range ($\|i-j\| \leq 5$)	46
long-range ($\|i-j\| > 5$)	0
no. of hydrogen bonds (as restraints)	5 (10)
no. of dihedral angle (ϕ) restraints	6
X-PLOR energies (kJ/mol)	
E_{total}	55.31 ± 0.27
E_{NOE}	4.88 ± 0.22
$E_{dihedral}$	0
rmsd from idealized covalent geometry	
bonds (Å)	0.002191 ± 0.000047
angles (deg)	0.6039 ± 0.0010
impropers (deg)	0.3848 ± 0.0043
Ramachandran plot (%)	
most favored	75.0
additional allowed	23.5
generously allowed	1.5
disallowed region	0
pairwise atomic rmsd (Å)	
well-defined region (residues 11−27)	
backbone heavy atoms	0.65 ± 0.22
all heavy atoms	0.91 ± 0.21

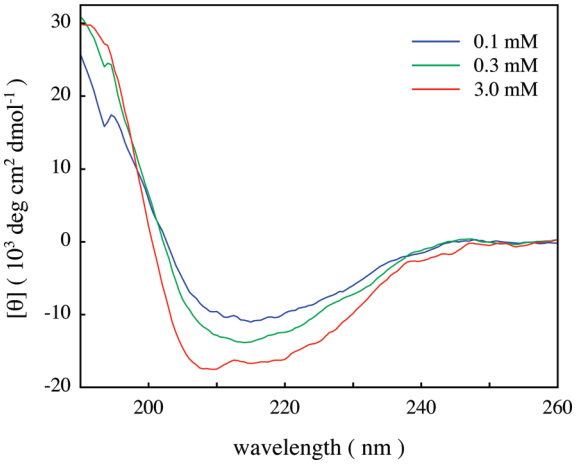

FIGURE 1: Far-ultraviolet CD spectra of big-N. The spectra of big-N were recorded at 30 °C in 0.1 (blue), 0.3 (green), and 3.0 mM SDS (red).

RESULTS

CD Experiments. The CD spectrum of big-N in the presence of SDS showed a negative minimum at 205−220 nm and a positive ellipticity below 200 nm. These features of the spectra were enhanced as SDS was added to the solution (Figure 1), suggesting that big-N peptide becomes more structured in the presence of SDS. Considering that the spectrum at 10 mM SDS was essentially superimposed on that at 3.0 mM SDS (data not shown), the structure formation of big-N reached a plateau below 3.0 mM SDS. Thus, the structure of big-N appears to be induced in micellar environments and to be in equilibrium at > 3.0 mM SDS. When we used DPC that is a milder detergent than SDS and has a phosphate headgroup, DPC also induced a similar alteration in the CD spectra in a concentration-dependent manner, and the shape of spectrum at 10 mM DPC was identical to that at 1.0 mM SDS (data not shown). Therefore, the α-helix formation of big-N is not likely to be caused by a simple α-helix-inducing effect of SDS.

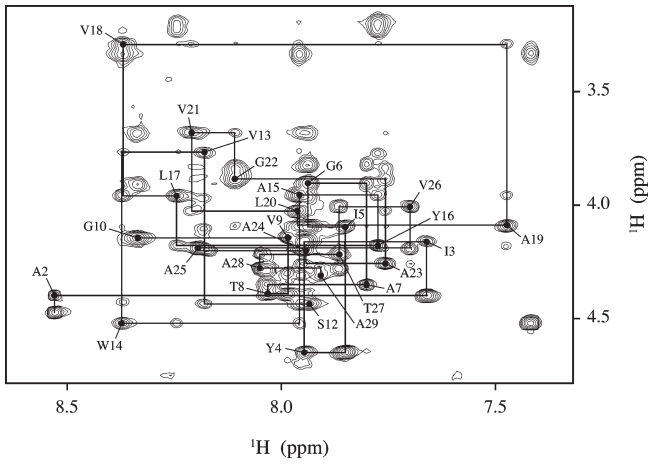

FIGURE 2: Fingerprint region of the NOESY spectrum for big-N in 100 mM SDS-d_{25}. Filled circles indicate the positions of $^1H^N-^1H^\alpha$ cross-peaks, and straight lines demonstrate the sequential connectivities.

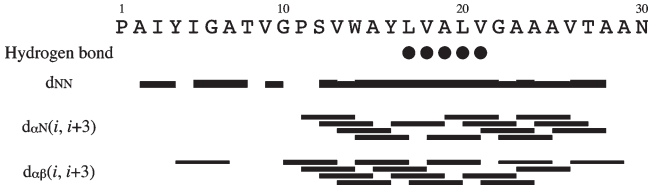

FIGURE 3: Summary of NOE connectivities that are characteristic of an α-helix structure. NOESY spectra were acquired with a mixing of 120 ms in a 5 or 100% D_2O solution. The thickness of the lines represents the relative intensity of the corresponding NOE cross-peak; e.g., thick lines indicate relatively strong peaks. A dot under the amino acid sequence indicates a slowly exchanging amide proton used as hydrogen bond information in the structure calculation of big-N.

Solution Structure of Big-N in SDS Micelles. The obtained NMR spectra were of sufficient quality to analyze and calculate the solution structure of big-N (Figure 2). Sequence-specific assignments for all backbone amide protons were achieved by using the two-dimensional TOCSY and NOESY spectra. The assignment of the cross-peaks on the NOESY spectra showed the presence of secondary structure in the big-N molecule (Figure 3). Some characteristic NOE connectivities were detected in the C-terminal half of big-N (residues G10−A29). The $d_{\alpha N}(i,i+3)$ and $d_{\alpha\beta}(i,i+3)$ patterns distinctly indicate that the G10−A29 region of big-N adopts a single α-helix conformation in SDS micelles. This region includes residues L17−V21 possessing amide protons that exchanged slowly with the solvent deuterium. In addition, the region of residues Y4−A7 gave an NOE signal that is diagnostic of α-helix formation, $d_{\alpha\beta}(i,i+3)$, implying that an additional helical conformation is present in the N-terminal half of big-N. The N-terminal region, including this helical conformation, is expected to project away from the C-terminal α-helix as no long-range NOE was found between the N-terminal and C-terminal regions (Table 1).

The solution structure of big-N was obtained from structure calculations using a total of 266 NOE-derived distance restraints, five hydrogen bonds (as 10 distance restraints), and 6 dihedral angle (ϕ) restraints (Figure 4A). For the 20 selected conformers with the lowest energy, residues P11−T27 were relatively well-defined with a backbone root-mean-square deviation (rmsd) of 0.65 ± 0.22 Å (Table 1). According to the Ramachandran plot, all residues (except for glycine and proline) were within the

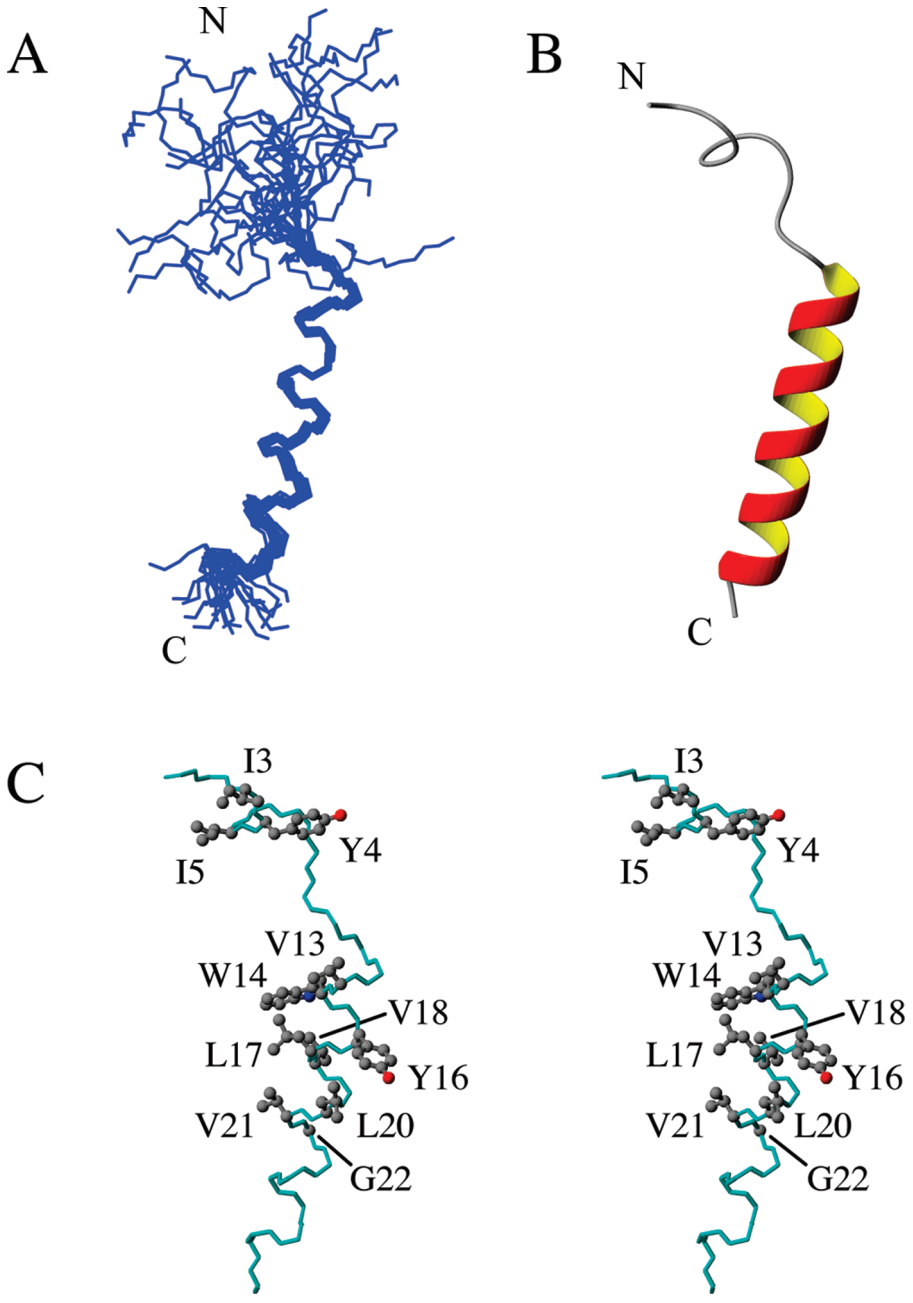

FIGURE 4: Solution structure of big-N in 100 mM SDS. (A) The backbone traces of the 20 lowest-energy structures are superimposed by using the backbone atoms (N, C^{α}, and C) for residues 11−27. (B) Ribbon representation of the energy-minimized average structure of big-N. (C) Stereoview of the energy-minimized average structure of big-N. The side chains mentioned in the text are shown with a ball-and-stick scheme.

allowable regions, with no distance restraints with a violation value larger than 0.20 Å or dihedral angle restraints with a violation.

The energy-minimized average structure of big-N peptide exhibited an α-helix structure spanning residues P11−A28 (Figure 4B). Despite the presence of a glycine residue (G22) in the middle of the α-helix, the overall helix is straight (Figure 4). A tryptophan (W14) and a tyrosine (Y16) residue are located in the N-terminal portion of the helix, and their side chains appear to be proximal to those of residues V18 and L20, respectively. An upfield shift of ^{1}H resonance was observed for $^1H^{\gamma 2}$ of V18 (0.42 ppm) in the former case, but not in the latter, indicating that the side chain of W14 is close to that of V18 such that the ring current effect of W14 affects the chemical shift of V18. However the ^{1}H resonances of L20 are not significantly affected by the aromatic ring of Y16, indicating a large distance between their side chains.

The C-terminal half of big-N peptide forms an α-helix structure, while the remaining N-terminal region is disordered except for residues I3−I5, which present some degree of local convergence (Figure S1 of the Supporting Information). Although residues I3, Y4, and I5 adopt irregular conformations, their hydrophobic side chains are directed to one side and arranged to form a flat surface (Figure 4C), implying an interface with the hydrophobic core of the SDS micelle.

NMR Experiments Using Paramagnetic Probes. To identify the interaction of big-N with SDS micelles, the effect of paramagnetic probes was estimated from two-dimensional TOCSY spectra with and without 16-Dox, Mn^{2+} ion, or Mn^{2+} and EDTA. EDTA chelates Mn^{2+} ion to form a $Mn(EDTA)^{2-}$ complex with a negative charge, thereby preventing electrostatic interactions between Mn^{2+} ions and the sulfate groups of SDS molecules. Cai et al. reported that a similar complex, $Ni(EDTA)^{2-}$,

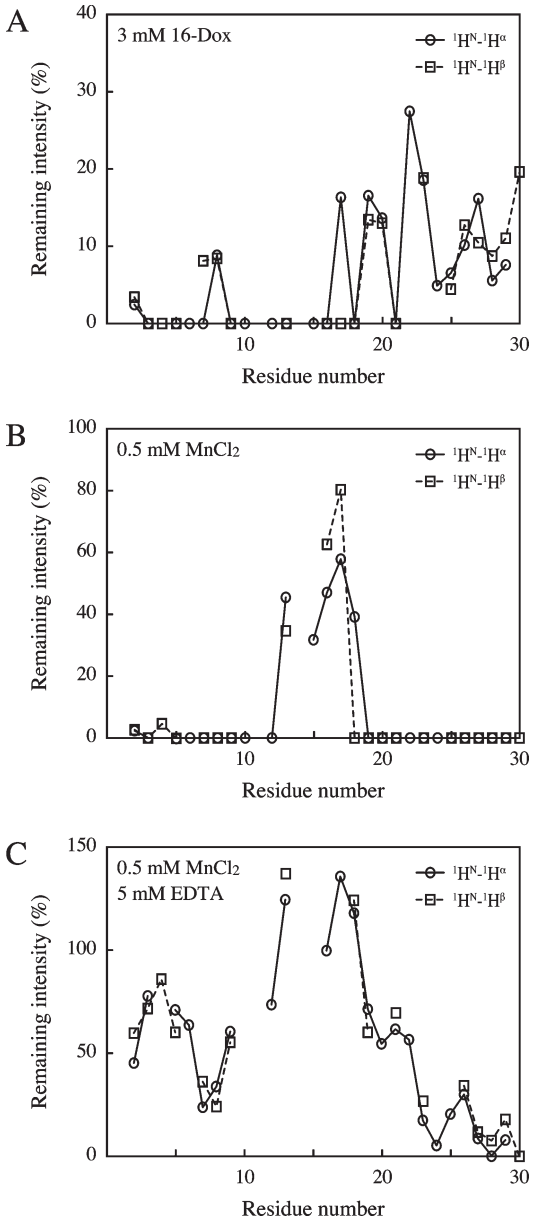

FIGURE 5: Comparison of the effect of paramagnetic probes on big-N in 100 mM SDS: 3 mM 16-Dox (A), 0.5 mM $MnCl_2$ (B), and 0.5 mM $MnCl_2$ and 5 mM EDTA (C). The intensity ratio of the cross-peaks, $^1H^N-^1H^\alpha$ (—○—) and $^1H^N-^1H^\beta$ (---□---), with and without the paramagnetic probes, is plotted along the amino acid sequence. The signal with a serious overlap was excluded from the analysis.

interacts with proteins via electrostatic interactions and induces signal broadening (*30*). However, nonspecific contacts between big-N and the $Mn(EDTA)^{2-}$ complex may be ignored because big-N has a highly hydrophobic sequence without charged residues.

In the presence of 3 mM 16-Dox, the remaining intensity of the amide cross-peaks is shown in Figure 5A. All residues were significantly affected by the addition of 16-Dox, and the signal intensity was decreased to 30% of the original level even in the cross-peak with the least attenuation. However, many cross-peaks were barely detectable in a small portion of the N-terminal half (residues A7 and T8) and the C-terminal half of big-N. On the other hand, the addition of 0.5 mM Mn^{2+} ion gave different results for the remaining intensity plot (Figure 5B). As expected, the pattern of the plot obtained by the addition of Mn^{2+} ion appears to have a complementary relationship to that obtained

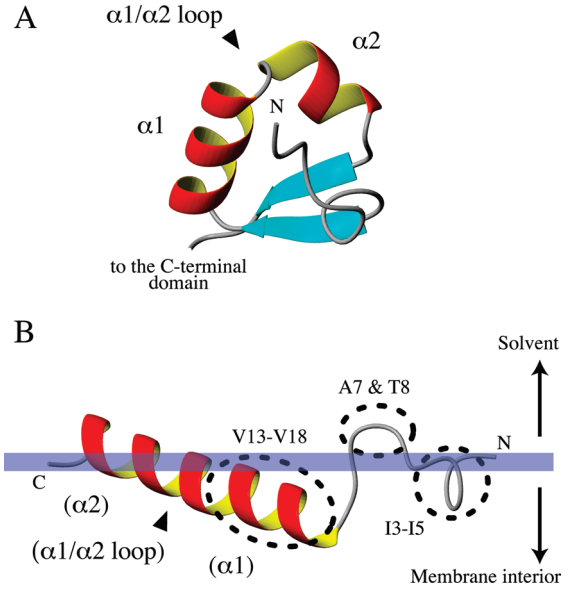

FIGURE 6: Conformational change in the N-terminal domain of big defensin with and without micelles. (A) Close-up view of the N-terminal domain of big defensin. This structure was determined in solution without micelles (*19*). (B) Model illustrating the insertion of big-N into the target membrane. The location of the residues mentioned in the text is denoted with dashed lines.

by the addition of 16-Dox. Many cross-peaks completely disappeared in the presence of Mn^{2+} ion, except for residues Y4 and V13−V18. In this case, the cross-peak of Y4 was observed at a level comparable to the spectral noise, whereas those derived from residues V13−V18 were clearly detectable, suggesting that the V13−V18 region, located in the N-terminal half of the α-helix structure, is effectively protected from Mn^{2+} ions. Moreover, the supplemental EDTA obviously improved the signal survival in the presence of Mn^{2+} (Figure 5C). The cross-peaks of residues A2−G6 and V9−G22 remained at levels more than 50% greater than the original intensities, while substantial signal suppression was found for residues A7, T8, and A23−N30. Thus, a portion around residues I3−I5 also has a tendency to be protected from Mn^{2+} ions.

DISCUSSION

CD and NMR analyses using the N-terminal fragment of big defensin, big-N, showed that the big-N peptide forms a single α-helix structure, spanning residues P11−A28, in the micellar environment. A previous study revealed that the N-terminal domain of the full-length big defensin adopts a compact globular conformation, including a parallel β-sheet and two α-helices, α1 (residues P11−L21, numbered according to the big-N peptide) and α2 (residues A23−A28), in the absence of micelles (Figure 6A) (*19*). These α1 and α2 helices are connected by a short loop and make an acute angle. The α1 helix out of the first β-strand projects away from the β-sheet, while the α2 helix is oriented toward the β-sheet and followed by the second β-strand. Thus, the presence of the α1−α2 loop and the β-sheet appears to contribute to the formation of the globular N-terminal domain of big defensin. Taken together, these two α-helices of big defensin, α1 and α2, appear to combine and extend straight in micellar environments, resulting in a single α-helix corresponding to the big-N structure resolved in this study (Figure 6B). These findings support a previous report that the parallel β-sheet in the N-terminal domain of big defensin is disrupted in the presence

of micelles (*19*). Therefore, the structural change in the N-terminal domain of big defensin described here is not caused by peptide fragmentation but reflects the essential nature of big defensin.

NMR experiments using paramagnetic probes elucidated the location of peptides on the membrane surface. In micellar systems, signal attenuation induced by 16-Dox or Mn^{2+} ion indicates that the corresponding amino acid is buried in the interior of the micelle or is exposed to solvent, respectively (*31*). In our study, the attenuation profile in the presence of 16-Dox or Mn^{2+} consistently showed that the N-terminal half of the α-helix and residues I3−I5 of big-N peptide contact SDS micelles, while the C-terminal half of the α-helix and residues A7 and T8 are exposed to solvent (Figure 6B). Residues V13−V18, in particular, exhibited strong exclusion from Mn^{2+} ions, implying that this region is completely buried in the interior of the micelle and interacts with its hydrophobic core. Residues I3−I5 also exhibited a preference for micellar environments rather than the solvent. However, the signal attenuations of residues I3−I5 upon addition of Mn^{2+} ion were significantly smaller than those of residues V13−V18, and the cross-peaks derived from residues I3−I5 were hardly detected in the presence of Mn^{2+} ions alone. Thus, residues I3−I5 are most likely located in the micellar interface in which the sulfate groups of SDS molecules are most frequently found. Considering that the side chains of residues I3−I5 are arranged as a flat surface, it is likely that they face the hydrophobic core, whereas the backbone is located in the interface region.

These micelle and membrane partitioning properties of big-N peptide are rationally explained by the "interfacial hydrophobicity scale" (ΔG_{IF}), which presents the free energies of the transfer of each amino acid in unfolded peptide from solvent to the membrane interface (*32*, *33*). According to this scale, hydrophobic amino acids such as Ile, Leu, Trp, and Tyr are preferentially located in the interfacial region rather than in solvent. In addition, the "octanol-interface scale" ($\Delta G_{oct\text{-}IF}$) can estimate the preference of an amino acid for the hydrophobic core of the membrane as an α-helix relative to the interface as an unfolded chain, indicating that aliphatic amino acids such as Ile, Leu, and Val belong to a group strongly preferring the hydrophobic core (*34*). In big-N peptide, those amino acids with a larger negative value of ΔG_{IF} and $\Delta G_{oct\text{-}IF}$ are frequently located in regions that present protection from Mn^{2+} ions, i.e., residues I3−I5 and the N-terminal half of the α-helix (Figure S2 of the Supporting Information). It seems likely that the aromatic residues, Y4, W14, and Y16, which have a remarkably small ΔG_{IF} compared with those of other amino acids, predominantly contribute to the partitioning of big-N to the micellar interface, while the aliphatic residues around the aromatic residues, I3, I5, V13, L17, V18, L20, and V21, with a larger negative value of $\Delta G_{oct\text{-}IF}$, induce deeper penetration into the hydrophobic core of the micelle. In addition, residues V13, W14, Y16, L17, V18, L20, and V21 are located on one face of the α-helix to form a surface favorable for making contacts with the hydrophobic core of the membrane (Figure 4C). Taken together, the N-terminal half of the α-helix dips in the membrane interior through membrane-preferring residues, whereas the C-terminal half is exposed to solvent (Figure 6B).

Antimicrobial peptides with penetration behavior similar to that of big-N are produced by lactic acid bacteria, and they are termed pediocin-like bacteriocins (*10*, *11*). Pediocin-like bacteriocins have an α-helix followed by an extended C-terminal tail that folds back onto the α-helix, thereby creating a hairpinlike structure penetrating into the hydrophobic core of the membrane. The association between the hairpinlike structure and the membrane plays an essential role in the antimicrobial activities of the bacteriocins, as the region of the hairpinlike structure determines the target specificity and bactericidal activity (*13*, *35*). In addition, the oblique insertion of the α-helix contributes to destabilization of the membrane structure and an increase in the extent of permeabilization (*13*, *36*). In the case of big-N, the α-helix inserts into the membrane with a dipping N-terminal edge, whereas residues A7 and T8 leading to the α-helix are exposed to solvent (Figure 6B). This membrane integration topology of big-N implies the presence of a hairpin-like or turn conformation in the N-terminus, and not in the C-terminus, of the α-helix. Thus, the insertion of the α-helix into the target membrane might be involved in the antimicrobial activity of big defensin against Gram-positive bacteria. Although further experimental evidence is needed to completely understand the bactericidal action of big defensin, this study proposes a novel model by which big defensin suppresses Gram-positive pathogens: big defensin dramatically changes its N-terminal structure to provide a scaffold for associating with the target membrane.

SUPPORTING INFORMATION AVAILABLE

Local rmsd plot for the backbone atoms of the 20 selected structures of big-N and plot of the free energies for transferring amino acids from the solvent to the membrane interface and from the interface to the hydrophobic core of the membrane. This material is available free of charge via the Internet at http://pubs.acs.org.

REFERENCES

1. Bulet, P., Stöklin, R., and Menin, L. (2004) Anti-microbial peptides: From invertebrates to vertebrates. *Immunol. Rev. 198*, 169–184.
2. Hancock, R. E. W., Brown, K. L., and Mookherjee, N. (2006) Host defense peptides from invertebrates: Emerging antimicrobial strategies. *Immunobiology 211*, 315–322.
3. Ganz, T. (2003) Defensins: Antimicrobial peptides of innate immunity. *Nat. Rev. Immunol. 3*, 710–720.
4. Selsted, M. E., and Ouellette, A. J. (2005) Mammalian defensins in the antimicrobial immune response. *Nat. Immunol. 6*, 551–557.
5. Lohner, K., and Prenner, E. J. (1999) Differential scanning calorimetry and X-ray diffraction studies of the specificity of the interaction of antimicrobial peptides with membrane-mimetic systems. *Biochim. Biophys. Acta 1462*, 141–156.
6. Kagan, B. L., Selsted, M. E., Ganz, T., and Lehner, R. I. (1990) Antimicrobial defensin peptides form voltage-dependent ion-permeable channels in planar lipid bilayer membranes. *Proc. Natl. Acad. Sci. U.S.A. 87*, 210–214.
7. Fujii, G., Selsted, M. E., and Eisenberg, D. (1993) Defensins promote fusion and lysis of negatively charged membranes. *Protein Sci. 2*, 1301–1312.
8. Wimley, W. C., Selsted, M. E., and White, S. H. (1994) Interactions between human defensins and lipid bilayers: Evidence for formation of multimeric pores. *Protein Sci. 3*, 1362–1373.
9. Lohner, K., Latal, A., Lehrer, R. I., and Ganz, T. (1997) Differential scanning microcalorimetry indicates that human defensin, HNP-2, interacts specifically with biomembrane mimetic systems. *Biochemistry 36*, 1525–1531.
10. Nes, I. F., Holo, H., Fimland, G., Hauge, H. H., and Nissen-Meyer, J. (2002) Unmodified peptide-bacteriocins (class II) produced by lactic acid bacteria. In Peptide Antibiotics: Discovery, Modes of Action and Application (Dutton, C., Haxell, M., McArthur, H., and Wax, R. G., Eds.) Marcel Dekker, Inc., New York.
11. Fimland, G., Johnsen, L., Dalhus, B., and Nissen-Meyer, J. (2005) Pediocin-like antimicrobial peptides (class IIa bacteriocins) and their immunity proteins: Biosynthesis, structure, and mode of action. *J. Pept. Sci. 11*, 688–696.

12. Fimland, G., Blingsmo, O. R., Sletten, K., Jung, G., Nes, I. F., and Nissen-Meyer, J. (1996) New biologically active hybrid bacteriocins constructed by combining regions from various pediocin-like bacteriocins: The C-terminal region is important for determining specificity. *Appl. Environ. Microbiol. 62*, 3313–3318.
13. Fimland, G., Eijsink, V. G. H., and Nissen-Meyer, J. (2002) Mutational analysis of the role of tryptophan residues in an antimicrobial peptide. *Biochemistry 41*, 9508–9515.
14. Iwanaga, S., Kawabata, S., and Muta, T. (1998) New types of clotting factors and defense molecules found in horseshoe crab hemolymph: Their structures and functions. *J. Biochem. 123*, 1–15.
15. Iwanaga, S. (2002) The molecular basis of innate immunity in the horseshoe crab. *Curr. Opin. Immunol. 14*, 87–95.
16. Toh, Y., Mizutani, A., Tokunaga, F., Muta, T., and Iwanaga, S. (1991) Morphology of the granular hemocytes of the Japanese horseshoe crab *Tachypleus tridentatus* and immunocytochemical localization of clotting factors and antimicrobial substances. *Cell Tissue Res. 266*, 137–147.
17. Chaby, R. (2004) Lipopolysaccharide-binding molecules: Transporters, blockers and sensors. *Cell. Mol. Life Sci. 61*, 1697–1713.
18. Saito, T., Kawabata, S., Shigenaga, T., Takayenoki, Y., Cho, J., Nakajima, H., Hirata, M., and Iwanaga, S. (1995) A novel big defensin identified in horseshoe crab hemocytes: Isolation, amino acid sequence, and antimicrobial activity. *J. Biochem. 117*, 1131–1137.
19. Kouno, T., Fujitani, N., Mizuguchi, M., Osaki, T., Nishimura, S., Kawabata, S., Aizawa, T., Demura, M., Nitta, K., and Kawano, K. (2008) A novel β-defensin structure: A potential strategy of big defensin for overcoming resistance by Gram-positive bacteria. *Biochemistry 47*, 10611–10619.
20. Pace, C. N., Vajdos, F., Fee, L., Grimsley, G., and Gray, T. (1995) How to measure and predict the molar absorption coefficient of a protein. *Protein Sci. 4*, 2411–2423.
21. Rance, M., Sørensen, O. W., Bodenhausen, G., Wagner, G., Ernst, R. R., and Wuthrich, K. (1983) Improved spectral resolution in COSY ^{1}H NMR spectra of proteins via double quantum filtering. *Biochem. Biophys. Res. Commun. 117*, 479–485.
22. Braunschweiler, L., and Ernst, R. R. (1983) Coherence transfer by isotropic mixing: Application to proton correlation spectroscopy. *J. Magn. Reson. 53*, 521–528.
23. Kumar, A., Ernst, R. R., and Wuthrich, K. (1980) A two-dimensional nuclear Overhauser enhancement (2D NOE) experiment for the elucidation of complete proton-proton cross-relaxation networks in biological macromolecules. *Biochem. Biophys. Res. Commun. 9*, 1–6.
24. Sklenar, V., Piotto, M., Leppik, R., and Saudek, V. (1993) Gradient-tailored water suppression for ^{1}H-^{15}N HSQC experiments optimized to retain full sensitivity. *J. Magn. Reson., Ser. A 102*, 241–245.
25. Wuthrich, K. (1986) NMR of Proteins and Nucleic Acid , John Wiley & Sons Inc., New York.
26. Delaglio, F., Grzesiek, S., Vuister, G. W., Zhu, G., Pfeifer, J., and Bax, A. (1995) NMRPipe: A multidimensional spectral processing system based on UNIX pipes. *J. Biomol. NMR 6*, 277–293.
27. Goddard, T. D., and Kneller, D. G. (2005) Sparky 3 , University of California, San Franciso.
28. Koradi, R., Billeter, M., and Wuthrich, K. (1996) MOLMOL: A program for display and analysis of macromolecular structures. *J. Mol. Graphics 14*, 51–55.
29. Laskowski, R. A., Rullman, J. A., MacArthur, M. W., Kaptein, R., and Thornton, J. M. (1996) AQUA and PROCHECK-NMR: Programs for checking the quality of protein structures solved by NMR. *J. Biomol. NMR 8*, 477–486.
30. Cai, S., Seu, C., Kovacs, Z., Sherry, D., and Chen, Y. (2006) Sensitibity enhancement of multidimensional NMR experiments by paramagnetic relaxation effects. *J. Am. Chem. Soc. 128*, 13474–13478.
31. Damberg, P., Jarvet, J., and Gräslund, A. (2001) Micellar systems as solvents in peptide and protein structure determination. *Methods Enzymol. 339*, 271–285.
32. Wimley, W. C., and White, S. H. (1996) Experimentally determined hydrophobicity scale for proteins at membrane interfaces. *Nat. Struct. Biol. 3*, 842–848.
33. White, S. H., and Wimley, W. C. (1998) Hydrophobic interactions of peptides with membrane interface. *Biochim. Biophys. Acta 1376*, 339–352.
34. White, S. H. (2003) Translocons, thermodynamics, and the folding of membrane proteins. *FEBS Lett. 555*, 116–121.
35. Johnsen, L., Fimland, G., and Nissen-Meyer, J. (2005) The C-termial domain of pediocin-like antimicrobial peptides (class IIa bacteriocins) is involved in specific recognition of the C-terminal part of cognate immunity proteins and in determining the antimicrobial spectrum. *J. Biol. Chem. 280*, 9243–9250.
36. Bennik, M. H. J., Vanloo, B., Brasseur, R., Gorris, L. G. M., and Smid, E. J. (1998) A novel bacteriocin with a YGNGV motif from vegetable-associated *Enterococcus mundtii*: Full characterization and interaction with target organisms. *Biochim. Biophys. Acta 1373*, 47–58.